

Discovery and Characterization of Gut Microbiota Decarboxylases that Can Produce the Neurotransmitter Tryptamine

Brianna B. Williams,¹ Andrew H. Van Benschoten,¹ Peter Cimermancic,¹ Mohamed S. Donia,¹ Michael Zimmermann,² Mao Takeuchi,¹ Atsushi Ishihara,³ Purna C. Kashyap,⁴ James S. Fraser,¹ and Michael A. Fischbach^{1,*}

¹Department of Bioengineering and Therapeutic Sciences and the California Institute for Quantitative Biosciences, University of California, San Francisco, San Francisco, CA 94158, USA

²ETH Zurich, Institute of Molecular Systems Biology, Zurich 8093, Switzerland

³Faculty of Agriculture, Tottori University, Koyama, Tottori 680-8550, Japan

⁴Mayo Clinic, 200 First Street SW, Rochester, MN 55905, USA

*Correspondence: fischbach@fischbachgroup.org

<http://dx.doi.org/10.1016/j.chom.2014.09.001>

SUMMARY

Several recent studies describe the influence of the gut microbiota on host brain and behavior. However, the mechanisms responsible for microbiota-nervous system interactions are largely unknown. Using a combination of genetics, biochemistry, and crystallography, we identify and characterize two phylogenetically distinct enzymes found in the human microbiome that decarboxylate tryptophan to form the β -arylamine neurotransmitter tryptamine. Although this enzymatic activity is exceedingly rare among bacteria more broadly, analysis of the Human Microbiome Project data demonstrate that at least 10% of the human population harbors at least one bacterium encoding a tryptophan decarboxylase in their gut community. Our results uncover a previously unrecognized enzymatic activity that can give rise to host-modulatory compounds and suggests a potential direct mechanism by which gut microbiota can influence host physiology, including behavior.

INTRODUCTION

It is becoming increasingly clear that the gut microbiota are important for nervous system function. In 1978, excessive levels of the intestinal hormone VIP (vasoactive intestinal peptide) were discovered in cerebrospinal fluid (Ebeid et al., 1978), establishing a connection between the gut and the brain. Over the past three decades, this relationship has expanded to include pathways in the autonomic and enteric nervous systems, the neuroendocrine system, and the immune system. More recently, the ability of the intestinal microbiota to modulate host neurological activity has become a focus of investigation. A 2004 study comparing germ-free and specific-pathogen-free mice demonstrated that the microbiota are required for the development of the hypothalamic-pituitary-adrenal (HPA) system, which is important for host stress response (Sudo et al., 2004). Additional studies showed

that the vagus nerve is a major communication pathway used by gut bacteria to influence neurochemistry and behavior (Bravo et al., 2011) and established a role for gut microbial colonization in modulating neuronal circuits involved in motor control and anxiety behavior (Diaz Heijtz et al., 2011). A recent paper from Mazmanian and coworkers used the maternal immune activation model of autism spectrum disorder to demonstrate a role for the microbiota in the development of autism and implicated a microbiota-derived metabolite, 4-ethylphenylsulfate, in its pathology (Hsiao et al., 2013). While it is now firmly established that the gut microbiota influence brain and behavior, the molecular mechanisms responsible for these phenomena have only begun to be explored.

In the work reported here, we had originally intended to characterize a pathway for the reductive metabolism of aromatic amino acids by the common gut Firmicute *Clostridium sporogenes*. In the course of carrying out preliminary experiments, we made the unexpected observation that *C. sporogenes* ATCC 15579 is capable of decarboxylating tryptophan (Trp) to tryptamine (Figure 1A), an activity that is exceedingly rare among bacteria. Here, we report the discovery and characterization of the *C. sporogenes* Trp decarboxylase, along with a phylogeny-informed screen of additional decarboxylases from the gut microbiota that led us to a second, unrelated Trp decarboxylase from another gut Firmicute, *Ruminococcus gnavus*. We then explore the structural determinants of Trp selectivity in the *R. gnavus* decarboxylase and show that at least 10% of the human population harbors one of these enzymes, opening the door to future efforts to explore their potential role in mediating a microbe-host interaction.

RESULTS

Clostridium sporogenes Decarboxylates Tryptophan to Tryptamine

We began with an interest in the reductive metabolism of aromatic amino acids by gut-associated species of *Clostridium*. In an effort to characterize the primary products to which tryptophan (Trp) was converted, we cultivated the common gut Firmicute *Clostridium sporogenes* ATCC 15579 in rich medium and then transferred the cell material into minimal medium to which

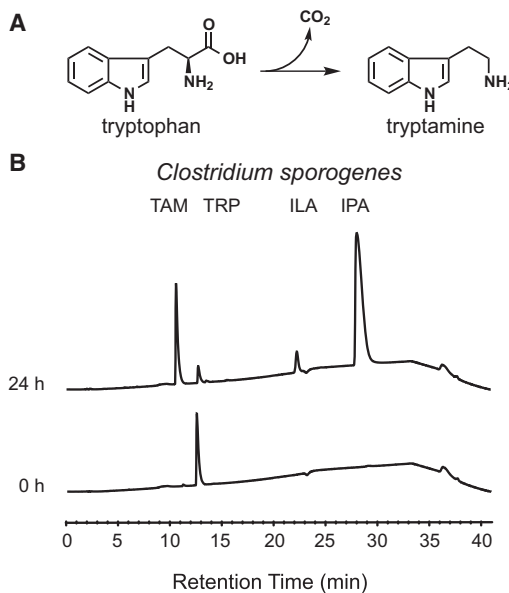


Figure 1. Tryptamine Production by *C. sporogenes*

(A) The proteinogenic amino acid L-tryptophan is decarboxylated to tryptamine, a biogenic amine neurotransmitter, by the action of pyridoxal phosphate (PLP)-dependent decarboxylases.

(B) Whole *C. sporogenes* were grown anaerobically in minimal media containing 5 g/L tryptophan and clarified supernatant was analyzed by HPLC. *C. sporogenes* converts tryptophan (12.5 min) into tryptamine (TAM, 10.5 min), indole lactic acid (ILA, 22 min), and indole propionic acid (IPA, 28 min). See also Figures S1 and S5.

Trp had been added. In extracts of these cultures, reverse-phase HPLC-MS analysis revealed an unexpected conversion product that was distinct from the known products of reductive Trp metabolism, indole lactic acid and indole propionic acid (Figure 1B). Since the mass of the unknown peak corresponded to the loss of the carboxylic acid group from Trp ($[M+H]^+$ *m/z*: calculated 161.22, observed 161.12), we tested and confirmed the identity of this compound to be tryptamine by coinjection with an authentic standard and by comparison of its ^1H NMR spectrum to that of an authentic standard (Figure S1A). Notably, the presence of tryptamine in the culture fluid of *C. sporogenes* indicated that tryptamine was not only being produced but also excreted from the cytoplasm to the extracellular space.

Identification of CLOSP0_02083 as a Trp Decarboxylase

We next set out to identify the enzyme responsible for Trp decarboxylation in *C. sporogenes* ATCC 15579. The two enzyme classes most commonly associated with amino acid decarboxylation are the pyridoxal 5'-phosphate (PLP)-dependent decarboxylases, in which the catalytic cycle begins with the covalent linkage of the substrate α -amine to PLP as a Schiff base (John, 1995; Schneider et al., 2000), and the pyruvoyl-dependent decarboxylases, in which a covalently bound pyruvoyl cofactor arises from an autocatalytic posttranslational modification (Gal-lagher et al., 1993; van Poelje and Snell, 1990). A computational search of the *C. sporogenes* ATCC 15579 genome sequence revealed three putative PLP-dependent decarboxylases, but no putative pyruvoyl-dependent enzymes.

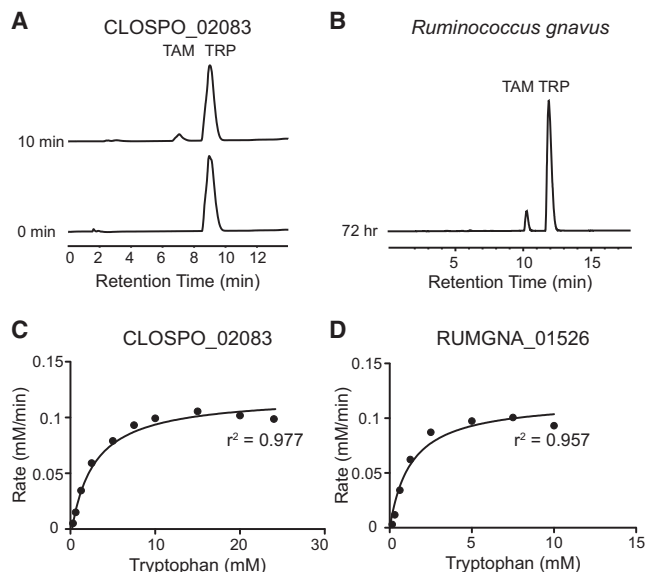


Figure 2. CLOSP0_02083 and RUMGNA_01526 Are Trp Decarboxylases

(A) Purified CLOSP0_02083 (100 nM) was incubated with 2.5 mM tryptophan for 10 min and quenched with 1 volume MeOH; 100 μl of the reaction mixture was analyzed by HPLC. The HPLC trace shows the conversion of tryptophan (TRP, 9 min) to tryptamine (TAM, 7 min).

(B) *R. gnavus* was grown anaerobically in minimal media containing 5 g/L tryptophan; 100 μl of the clarified supernatant was analyzed by HPLC. The HPLC trace shows the conversion of tryptophan (TRP, 12.5 min) to tryptamine (TAM, 10.9 min). Note: Different HPLC methods were used for (A) and (B).

(C and D) Rate (mM tryptamine/min) versus substrate concentration curves for tryptophan decarboxylation by (C) CLOSP0_02083 or (D) RUMGNA_01526. Enzyme was incubated with concentrations of tryptophan that varied from 0.15–24.5 mM. Error represents standard error of the mean. GraphPad was used to fit the Michaelis-Menten curve. See also Figure S2. Kinetic values are summarized in Figure S3.

None of the three genes were annotated as Trp decarboxylases; CLOSP0_02083 was predicted to be a tyrosine (Tyr) decarboxylase, while CLOSP0_03076 and CLOSP0_00504 were predicted to be glutamate decarboxylases. We began by characterizing CLOSP0_02083, hypothesizing that its annotation might be correct and Trp decarboxylation was a secondary activity—or incorrect but close, since Tyr and Trp are both aromatic amino acids. The CLOSP0_02083 gene was amplified by PCR from *C. sporogenes* genomic DNA, subcloned into the pET-28a expression vector, and heterologously overexpressed in *E. coli* BL21 (DE3) as an N-terminal His₆ fusion protein. CLOSP0_02083 fusion protein was purified by immobilized nickel affinity chromatography to > 95% homogeneity (Figure S1B). When CLOSP0_02083 was incubated with Trp for 6 min at 37°C, HPLC analysis of the reaction mixture revealed a new peak (Figure 2A). The identity of the corresponding compound was consistent with tryptamine by coelution with an authentic standard.

Kinetic Analysis of CLOSP0_02083 Activity with Aromatic Amino Acid Substrates

The previous result shows that CLOSP0_02083 is capable of decarboxylating Trp, but it does not rule out the possibility that one

of the other aromatic amino acids is transformed more efficiently. To gain insight into the substrate selectivity of CLOSPO_02083, we measured the basic kinetic parameters for CLOSPO_02083-catalyzed decarboxylation of the aromatic amino acids Trp, Tyr, and phenylalanine (Phe). To determine k_{cat} and K_m for CLOSPO_02083, the concentration of the amino acid substrate was varied under initial velocity conditions (Figures 2C and S4A). Trp is a robust substrate for decarboxylation CLOSPO_02083 with a K_m of 2.8 ± 0.0 mM, k_{cat} of 1200 min^{-1} and k_{cat}/K_m of $7.3 \times 10^3 \text{ M}^{-1}\text{sec}^{-1}$. The activity of CLOSPO_02083 against Phe was undetectable up to 90 mM substrate (Figure S1C). Although the limited solubility of Tyr prevented us from obtaining kinetic parameters, at the highest concentration of Tyr we tested, CLOSPO_02083 was 600-fold more efficient at decarboxylating Trp (Figure S1D). Collectively, these results show that Trp is accepted more efficiently as a substrate than Phe or Tyr.

These results suggest that the database annotation of CLOSPO_02083 as a Tyr decarboxylase is incorrect. The chemical distinction between Tyr and Trp is mild, since they are both aromatic amino acids. However, the biological distinction between their decarboxylation products is sharp: tyramine stimulates a pressor response that results in an increase in blood pressure (Bianchetti et al., 1982), whereas tryptamine induces the release of serotonin from enterochromaffin cells and stimulates GI motility (Takaki et al., 1985). Thus, a modest difference in a decarboxylase's substrate selectivity can lead to entirely distinct biological outcomes, placing a premium on biochemically characterizing the substrate selectivity of amino acid decarboxylases expressed by gut commensals.

A Phylogenetic Analysis of Bacterial Decarboxylases to Select a Functionally Diverse Set of 15 Candidate Enzymes

Several other gut-associated *Clostridium* spp. harbor a homolog of CLOSPO_02083, but this enzyme does not appear to be present in other gut Firmicutes. We next asked whether there exist additional unrelated Trp decarboxylases among the human microbiota. The only putative tryptophan decarboxylases in the NCBI databases come from plant and fungal genomes, but the fact that CLOSPO_02083 was misannotated as a Tyr decarboxylase led us to hypothesize that there might be other mis- or unannotated decarboxylases encoded by the microbiota that are Trp selective.

To select a small panel of candidate decarboxylases from the microbiota, we performed a phylogenetic analysis of bacterial decarboxylases in which protein sequences were grouped into clades in which members are predicted to share a similar (if not identical) substrate selectivity. We then chose 15 enzymes for characterization in a manner that maximized our ability to search the functional space of microbiome decarboxylases: at least one sequence from each of the largest clades and three additional sequences from smaller clades (Figure S2A). We obtained and cultivated each of the host organisms to isolate genomic DNA. The candidate decarboxylases were amplified by PCR, subcloned into the pET-28a expression vector, and heterologously overexpressed in *E. coli* BL21 as N-terminal His₆ fusion proteins.

A Phylogeny-Informed Screen for Additional Trp Decarboxylases from the Microbiota

Since our aim was to discover Trp decarboxylases rather than to obtain kinetic parameters for each enzyme in our screening panel, we developed and employed a whole-cell assay to rapidly assess the substrate selectivity of our candidate decarboxylases. *E. coli* BL21 (DE3) harboring candidate decarboxylases in pET-28a expression vectors were cultivated in rich medium and grown to stationary phase. The cells were transferred into minimal medium containing an aromatic amino acid substrate (Trp, Tyr, or Phe), and decarboxylation was monitored by analyzing cell-free culture fluid by analytical HPLC. This assay takes advantage of the fact that β-arylamines, the products of decarboxylase activity in the *E. coli* cytoplasm, could easily be detected in the extracellular fluid of *E. coli* cultures we screened and are not produced by wild-type *E. coli*.

An important limitation of the assay is that it is qualitative; in a manner that is likely due to differences in the level of active enzyme expressed, a more robust activity in the cell-based assay did not always translate into an enzyme with more efficient kinetic parameters. Moreover, we find that the assay detects low-level activities that may not be physiologically relevant, so a positive result only indicates the possibility of an activity and must be confirmed biochemically.

Nevertheless, our qualitative assay enabled us to rapidly screen 15 decarboxylases against three substrates (Figure S2B). One of the enzymes we screened, RUMGNA_01526, appeared to be capable of decarboxylating Trp robustly; notably, this enzyme was only very distantly related to CLOSPO_02083 (26% amino acid sequence identity). To confirm this result biochemically, we purified RUMGNA_01526 fusion protein by immobilized nickel affinity chromatography to >95% homogeneity (Figure S1B).

RUMGNA_01526 Is a Trp Decarboxylase

We measured the basic kinetic parameters for the decarboxylation of Trp, Tyr, and Phe by RUMGNA_01526. As shown in Figure 2D, Trp is a robust substrate for decarboxylation, with a k_{cat} of 4400 min^{-1} , a K_m of 1.1 ± 0.1 mM, and a k_{cat}/K_m of $6.8 \times 10^4 \text{ M}^{-1}\text{sec}^{-1}$. In spite of the robust activity of RUMGNA_01526 against Trp, Tyr, and Phe in the cell-based assay, the catalytic efficiency of RUMGNA_01526 for Trp is >1000-fold higher than it is for Phe (Figures 2D and S4B), due to the combination of a higher k_{cat} (19-fold) and a lower K_m (70-fold). Although the limited solubility of Tyr prevented us from obtaining kinetic parameters, at the highest concentration of Tyr we tested, RUMGNA_01526 was 1000-fold more efficient at decarboxylating Trp. These data suggest that tryptophan is the native substrate of RUMGNA_01526 (Figures S1C and S1D).

R. gnavus Excretes Tryptamine into the Extracellular Fluid

We showed above (Figure 1B) that *C. sporogenes* excretes the tryptamine generated by CLOSPO_02083 into the culture fluid. However, tryptamine produced in the cytoplasm could have a variety of alternative intracellular fates, including serving as a building block for the synthesis of a larger molecule. Having shown that RUMGNA_01526 is a Trp decarboxylase, we next asked whether *R. gnavus* excretes the tryptamine from RUMGNA_01526 into the extracellular space. We cultivated *R. gnavus* in rich medium until

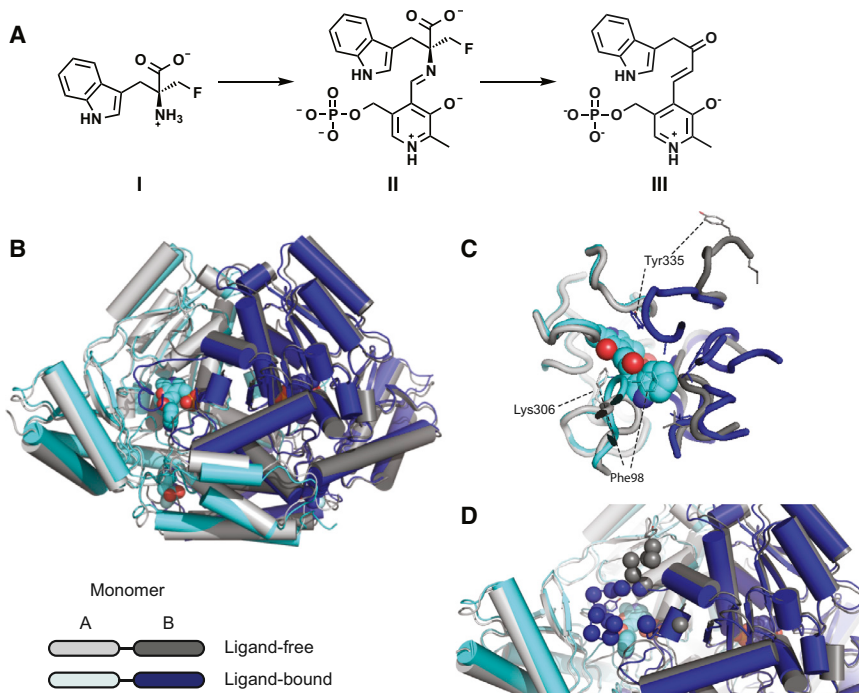


Figure 3. Crystal Structure of Apo and Ligand-bound RUMGNA_01526

(A) Schematic of proposed inhibitor mechanism: (S)- α -FMT (I) is converted to a PLP-(S)- α -FMT external aldimine intermediate (II), which undergoes decarboxylation, fluoride ion elimination, and transaldimination to form a PLP-(S)- α -FMT ketone adduct (III).

(B) Overlay of ligand-free (monomer A, light gray; monomer B, dark gray) and ligand-bound (monomer A, cyan; monomer B, blue) structures. In the active and allosteric sites, PLP-(S)- α -FMT and (S)- α -FMT (respectively) are shown in spheres.

(C) Active site with PLP-(S)- α -FMT bound reveals a repositioning of Tyr335 and Phe98. In the ligand-bound structure, Lys306 is no longer covalently bound to PLP.

(D) Upon engagement of (S)- α -FMT, residues 337–349 (dark blue spheres) fold over the active site, excluding solvent and forming critical interactions with the inhibitor. Dark gray spheres represent only ordered residues in apo structure. See also Figures S4 and S6.

stationary phase, transferred the cell material into a defined medium in the absence or presence of added Trp, and monitored the extracellular fluid by analytical HPLC. We observed that after 72 hr, the concentration of tryptamine reached \sim 1.7 mM (Figure 2B), showing that *R. gnavus* excretes tryptamine in vitro and suggesting that this strain has the potential to excrete tryptamine in the ecological setting of the gut lumen.

Tryptamine Induces Ion Secretion by Intestinal Epithelial Cells

The function of tryptamine in the context of microbe-host signaling in the gut is not well understood. As a starting point for exploring the physiology of tryptamine-mediated signaling, we performed an experiment to test whether tryptamine is capable of inducing ion secretion by intestinal epithelial cells. Using an Ussing chamber, a segment of proximal-mid murine colon mucosa was exposed to two concentrations of tryptamine and the change of short circuit current was measured. At 3 mM, a concentration comparable to the active concentration of other bacterial fermentation products such as short-chain fatty acids, tryptamine induced a significant change in short circuit current, confirming that it can affect colonic ion secretion (Figure S5). Since colonic ion secretion plays an important role in gastrointestinal motility, this result suggests that tryptamine-mediated signaling might affect the transit of food particles and bacterial cells through the gut lumen.

RUMGNA_01526 Is a Fold Type I PLP-Dependent Decarboxylase

We decided to use a combination of structural biology and phylogenetics to better understand the provenance of bacterial Trp decarboxylases. Crystals of CLOSP_02083 in the apo form failed to diffract to an adequate resolution, but we determined

the crystal structure of RUMGNA_01526 at 2.8 Å. The enzyme forms a dimer with 4565 Å² buried at the dimer interface. The active site is located at the dimer interface and therefore the enzyme is only functional in the dimeric state. The monomeric unit is comprised of three domains: an N-terminal domain containing three parallel α helices that pack against the other monomer, a large domain comprised of a nine-stranded β sheet surrounded by nine α helices containing the PLP-binding site, and a smaller C-terminal domain comprised of a four-strand anti-parallel β sheet surrounded by three α helices (Figure 3B). The structure is nearly identical to the open form of human glutamate decarboxylase (GAD65), with an overall α -carbon RMSD of 1.07 Å (Fenalti et al., 2007). Similar comparisons can be made to human aromatic amino acid decarboxylase (Giardina et al., 2011) and wild boar DOPA decarboxylase (Burkhard et al., 2001), with α -carbon RMSDs of 1.21 Å and 1.23 Å, respectively. The agreement between these structures highlights the commonality of this enzymatic fold, even across multiple species.

(S)- α -Fluoromethyltryptophan Is an Inhibitor of RUMGNA_01526

The close structural relationship between RUMGNA_01526 and glutamate decarboxylase raises the question of how the structural scaffold of RUMGNA_01526 accommodates the large, hydrophobic substrate Trp. Since the ideal approach to answering this question would involve determining the structure of RUMGNA_01526 bound to a Trp-mimicking inhibitor, we proceeded to determine whether a previously reported inhibitor of plant Trp decarboxylase, (S)- α -fluoromethyltryptophan [(S)- α -FMT; Figure 3A, I], was an inhibitor of RUMGNA_01526 (Ishihara et al., 2011).

Although mechanistic studies have not been performed to determine the mode of Trp decarboxylase inhibition by

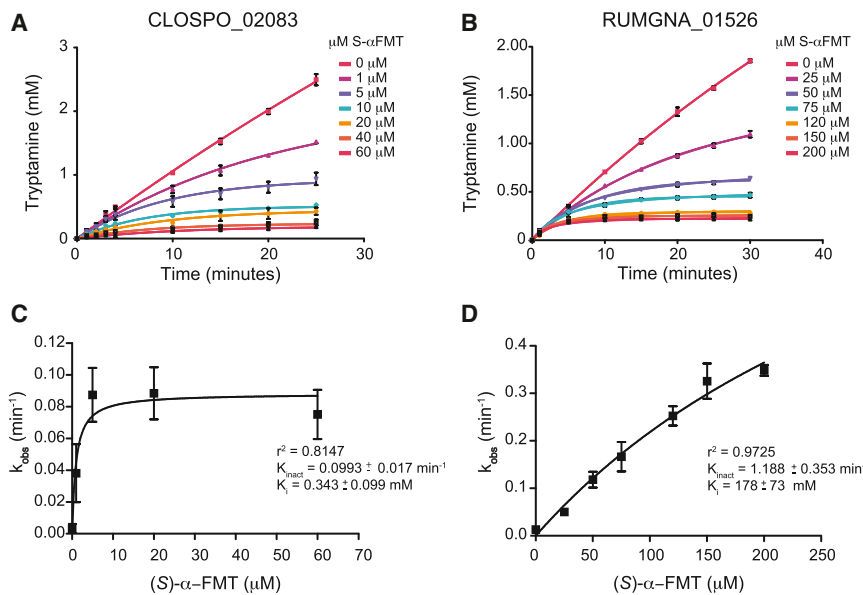


Figure 4. Decarboxylase Inhibition by (S)- α -FMT

Progress curve of tryptamine production by (A) CLOSP0_02083 and (B) RUMGNA_01526 in the presence of (A) 10 mM or (B) 2.5 mM tryptophan at various concentrations of inhibitor. Data were fit to the equation described in *Supplemental Experimental Procedures* to obtain k_{obs} .

(C and D) Plot of k_{obs} versus $[I]$. CLOSP0_02083 is inhibited more potently by (S)- α -FMT than RUMGNA_01526 due to a higher binding affinity of the inhibitor. Error represents standard error of the mean. See also Figure S3.

(S)- α -FMT, biochemical studies with a similar amino acid analog, (S)- α -fluoromethylhistidine ([S]- α -FMH), show that this inhibitor blocks histidine decarboxylase in a mechanism-dependent fashion that involves the formation of a covalent adduct between the inhibitor and PLP.

We measured the production of tryptamine by HPLC in the presence of various concentrations of inhibitor over 30 min and analyzed progress curves of the reaction to assess the kinetics of inhibition. Indeed, not only for RUMGNA_01526 but also for CLOSP0_02083, we observed progress curves in the presence of increasing concentrations of inhibitor, consistent with covalent inhibition (Figures 4A and 4B). Despite having a comparable K_m for Trp, RUMGNA_01526 has a weaker affinity for (S)- α -FMT than CLOSP0_02083 (K_i of 178 μ M versus 0.2 μ M). However, it is more rapidly inhibited (k_{inact} of 1.2 min^{-1} versus 0.1 min^{-1}), suggesting that once the weak enzyme-inhibitor complex forms, the relative orientation of PLP and the inhibitor is conducive to covalent bond formation (Figures 4C and 4D).

The inactivation of histidine decarboxylase by (S)- α -FMH is initiated by substrate decarboxylation followed by the elimination of fluoride ion (Bhattacharjee and Snell, 1990; Hayashi et al., 1986). A transaldimination releases the enamine, which can react and inactivate the PLP cofactor. In order to elucidate the mechanism by which (S)- α -FMT inhibits RUMGNA_01526, as well as to understand how RUMGNA_01526 accommodates the large, hydrophobic substrate Trp, we sought to determine the X-ray crystal structure of the inhibitor-bound enzyme.

A Key Loop Gates the Active Site and Contacts the Indole Side Chain of the Substrate Trp

We determined the crystal structure of inhibitor-bound RUMGNA_01526 at 2.8 Å. In the active site of the native enzyme, which is located in a cleft at the dimer interface, continuous electron density shows PLP covalently linked to K306 through a Schiff base. The major difference between the native and (S)- α -FMT-bound structures is the conformation of an extended loop (residues 337–349). The homologous loop was previously

identified as a major difference between GAD65 and GAD67, where differences in conformational dynamics are thought to be responsible for auto-inactivation of GAD65 (Fenalti et al., 2007). In porcine DOPA decarboxylase, this loop was disordered in three data sets from complexes with different inhibitors,

complicating structure-based drug design and an assessment of catalytic mechanisms (Burkhard et al., 2001). In contrast, we observed that when bound to PLP alone, this loop was partially disordered and the remaining ordered components jutted away from the active site, leaving the active site solvent-exposed. Upon engagement of (S)- α -FMT, electron density became clearer and the loop folded over the active site, excluding solvent and forming critical interactions with the inhibitor (Figure 3D). These data are consistent with a model in which loop 337–349 gates the active site, adopting a partially disordered, outward-facing conformation in the absence of substrate that enables access to the active site, and closing down to cap the active site after substrate entry.

Two other flexible loops within the active site of the inhibitor-bound enzyme are reordered to accommodate the indole side chain of (S)- α -FMT. In the absence of substrate, the first loop (residues 95–101) leaves the active site accessible for the entry of a substrate with a large aromatic side chain. Upon substrate binding, the loop conformational change places the phenyl ring of Phe98 directly above the π -system of the indole ring, stabilizing the inhibitor through a π -stacking interaction (Figure 3C). This loop appears to be a critical element for defining substrate selectivity; consistent with this possibility, it is conserved among decarboxylases in several related Firmicutes (discussed below). The second loop, residues 329–336, reorients to shift the phenolic side chain of Tyr335 closer to the active site, increasing the hydrophobicity of the substrate-binding pocket.

Insights into the Mechanism of Inhibition by (S)- α -FMT and a Potential Allosteric Site

In the inhibitor-bound structure, (S)- α -FMT has been decarboxylated; however, it has not been defluorinated as seen in the mechanism of (S)- α -FMH inhibition of histidine decarboxylase and remains covalently linked to PLP. This is supported by the absence of a suitable nucleophile in the active site that could be covalently modified by the defluorinated (S)- α -FMT-PLP adduct.

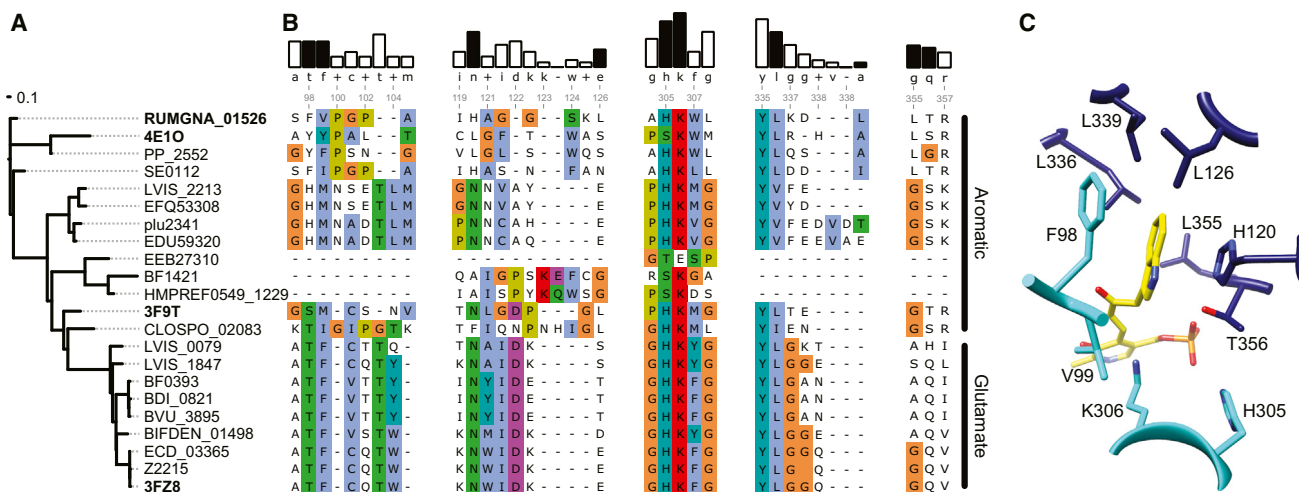


Figure 5. Sequence and Structural Analysis of Aromatic Amino Acid Decarboxylases

(A) The dendrogram on the left shows the degree of sequence similarity between various decarboxylases.
 (B) Alignment of select amino acid decarboxylases are numbered according to the RUMGNA_01526 sequence. Four structural components of RUMGNA_01526 important for substrate binding are highlighted. The bars above consensus sequence show the degree of sequence conservation; residues from the RUMGNA_01526 structure that interact (black bars) or do not interact (white) with the tryptophan substrate are indicated. Residues in the sequence alignment are colored according to the Clustal color code (http://ekhidna.biocenter.helsinki.fi/pfam2/clustal_colours).
 (C) RUMGNA_01526 active site showing residues represented by black bars in (B).

The (S)- α -FMT-PLP adduct (Figure 3A, III) is relatively disordered in the electron density maps of both active sites; however, the maps show an absence of density consistent with a covalent linkage between PLP and the enzyme. To further probe the identity of the adduct, we denatured the enzyme after incubation with PLP and (S)- α -FMT and analyzed the released product (Figure S10). We found a single species of mass 403, which most likely represents the ketone formed after (S)- α -FMT is decarboxylated, defluorinated, and deaminated (Figure S10, IV). The same adduct is also found during the inactivation of histidine decarboxylase by (S)- α -fluoromethylhistidine (Bhattacharjee and Snell, 1990). Collectively, these data indicate that the PLP-(S)- α -FMT adduct is formed and remains tightly bound rather than diffusing out of the active site. Thus, the blockade of RUMGNA_01526 by (S)- α -FMT appears to be an enzyme-catalyzed inactivation of the PLP coenzyme and does not involve a chemical modification of the enzyme itself.

Surprisingly, we observed an additional molecule of (S)- α -FMT bound to a site \sim 20 Å from the active site (Figure S4C). The inhibitor fits inside a hydrophobic pocket that is formed by the movement of an N-terminal loop (residues 16–22) and makes hydrogen bonds to S105 and the backbone of P102. While this binding event might be a crystallization artifact, the kinetic data are consistent with the possibility of cooperative substrate binding to an allosteric site as evidenced by a slight increase in the r^2 value for the fit to the Hill equation (Hill coefficient = 1.87) versus the Michaelis-Menten equation (Figures S3, S4A, and S4B).

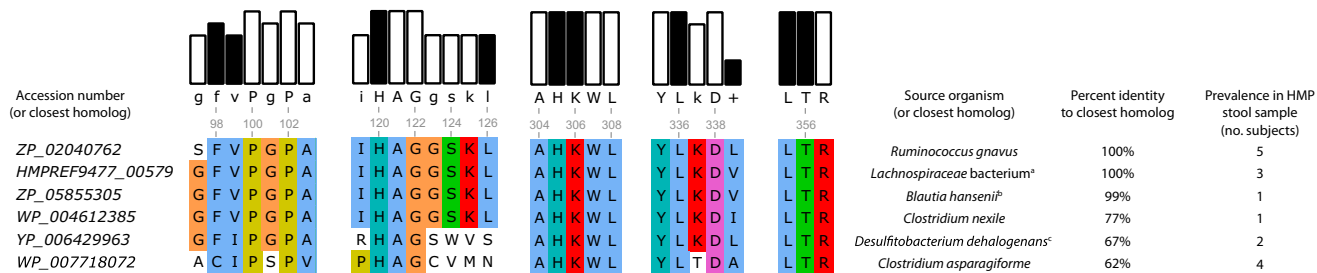
Evolutionary Insights from Sequence and Structure into the Substrate Selectivity and Origins of Bacterial Trp Decarboxylases

To better understand the mechanisms underlying the substrate recognition and specificity, we next aligned the amino acid se-

quences of 21 enzymes: 15 decarboxylases from the phylogeny-informed screen, 3 annotated histidine decarboxylases, and 3 decarboxylases with known structure. Three notable patterns are apparent from the multiple sequence alignment. First, while the multiple sequence alignment shows a high degree of similarity between the amino-acid substrate binding sites of the glutamate decarboxylases, the binding sites that accommodate aromatic amino-acid substrates differ significantly (Figure 5). With the exception of one enzyme (EEB27310), the only residue shared by all the sequences is K306, the active site lysine residue involved in binding PLP. Second, no apparent rules were found in the sequence alignment of the decarboxylases with aromatic amino acids as substrates that could explain their specificities or promiscuities for the aromatic amino acids; therefore, it is likely that the aromatic amino acid substrate specificity is governed by differences in the active site structures and/or orientations of the substrates. Even the serine residue at position 356 (354 in the original sequence) that was found to determine the histidine specificity of the human histidine decarboxylase (Komori et al., 2012) is found in other decarboxylases with no observed histidine activity (data not shown). Third, the binding sites of decarboxylases with aromatic amino acid substrates are rich in proline residues, suggesting that the specificity for different aromatic amino acid substrates could also be driven by active sites whose shapes match more rigidly those of the substrates.

Trp Decarboxylases Are Present in At Least 10% of the Samples from the NIH Human Microbiome Project

Initial assemblies of sequenced human stool samples from 86 healthy subjects were examined for the presence of similar amino acid decarboxylases. We used BLASTP to search the metagenomic contigs for homologs of RUMGNA_01526. In total,

**Figure 6. Presence of Tryptophan Decarboxylase in the Human Microbiome Project Samples**

Accession numbers of proteins of highest sequence identity to RUMGNA_01526 (ZP_02040762). BLAST percent identity was calculated for at least 100 amino acids. Fifteen subjects were found to contain homologs of the putative tryptophan decarboxylases. Of those, two contained 2 different homologs, and 13 contained one homolog. One subject harbored a gene with 93% identity to either ZP_0204072 from *R. gnatus* or HMPREF9477_00579 from *Lachnospiraceae* bacterium 2_1_58FAA. A sequence alignment is presented highlighting the residues identified by our structural analysis to be important for accommodating tryptophan (black bars). (a) *Lachnospiraceae* bacterium 2_1_58FAA, (b) *Blautia hansenii* DSM 20583, and (c) *Desulfobacterium dehalogenans* ATCC 51507.

we identified homologs of RUMGNA_01526 in 15 subjects (17% of the samples). Of those, 13 subjects contained only one decarboxylase homolog, while two subjects harbored two different homologs. Eight subjects (9.3%) contained a Trp decarboxylase homolog that is almost identical to the RUMGNA_01526 characterized here (>99% identical at the amino acid level over >100 residues). The rest of the samples harbored decarboxylase homologs that were 62%–93% identical to RUMGNA_01526 over >100 residues (Figure 6). Although further biochemical characterization is needed to assign these more distantly related homologs as aromatic amino acid decarboxylases, a sequence alignment to RUMGNA_01526 shows nearly 100% identity over the residues critical for accepting tryptophan (Figure 6). These homologs were highly similar to genes from a variety of anaerobic Firmicute reference genomes, such as *Clostridium asparagiforme*, *Clostridium nexile*, *Desulfobacterium dehalogenans*, and *Blautia hansenii*. Despite the fact that *C. sporogenes* ATCC 15579 is a human gut isolate, similar searches with CLOSP0_02083 yielded no hits. The presence of Trp decarboxylase homologs in 9%–17% of gut metagenomes of a random population of healthy humans suggests that tryptamine produced by gut bacteria may be more prevalent in humans than previously thought.

DISCUSSION

The production of tryptamine by *C. sporogenes* was notable for three reasons. First, while the decarboxylation of tryptophan to tryptamine is common in the plant kingdom (Facchini et al., 2000), Trp decarboxylation is an exceedingly rare activity among bacteria. To our knowledge, the only bacterial species in which this transformation is known are *Xenorhabdus nematophilus* and *Bacillus atrophaeus*, which are thought to produce tryptamine as a building block for the biosynthesis of larger natural products (Lang et al., 2008; Li et al., 1997; Proschak et al., 2011; Yuwen et al., 2013), and *Lactobacillus bulgaricus*, the only bacterial species known to excrete tryptamine (Chander et al., 1989).

Second, tryptamine is a β-arylamine neurotransmitter known to have a range of biological activities. As a trace amine found in low quantities in the brain, it is a ligand for the trace amine-associated receptors (TAARs) that potentiates the inhibitory response of cells

to serotonin (Borowsky et al., 2001; Zucchi et al., 2006), as well as a ligand for the sigma-2 receptor (Fontanilla et al., 2009). Moreover, tryptamine has been observed in human and rodent feces (Anderson, 1975; Brooks et al., 1984), where it is known to induce the release of serotonin by enterochromaffin cells (Takaki et al., 1985). Fluctuations in intestinal serotonin levels are thought to modulate GI motility (Lundgren, 1998; Turvill et al., 2000) and may play a role in the pathology of inflammatory bowel diseases (Bischoff et al., 2009; Linden et al., 2003, 2005). These findings are especially interesting in light of the critical role serotonin plays as a signaling molecule in the enteric nervous system (Mayer, 2011; Ormsbee and Fondacaro, 1985), where modulation of the serotonin receptors has been proposed as a treatment for irritable bowel syndrome (Gershon and Tack, 2007; Mawe et al., 2006). Indeed, the gut microbiome of IBS patients is often dominated by Firmicutes (Jeffery et al., 2012), the phylum from which the decarboxylases described here derive, raising the question of whether the bacterial production of tryptamine plays a role in the pathogenesis of IBS.

Third, tryptamine production represents a microbiota-mediated alteration in tryptophan metabolism. Host serotonin is produced from dietary tryptophan and metabolomic profiling has shown that germ-free mice have a 2.8-fold decrease in plasma serotonin over conventionalized mice, and elevated levels of tryptophan (Wikoff et al., 2009). Additionally, the level of tryptamine in feces increases by 200% in conventional versus germ-free mice (Marcobal et al., 2013) and there exist microbiota-derived tryptophan metabolites such as indole propionic acid in conventionalized but not germ-free mice (Wikoff et al., 2009). Three additional reports have shown that germ-free mice have elevated levels of tryptophan (Clarke et al., 2013; Diaz Heijtz et al., 2011; Desbonett et al., 2008) without explanatory changes in gene expression of tryptophan-utilizing enzymes and suggest that the microbiota are participating in tryptophan metabolism. Our discovery of tryptophan decarboxylases in the intestinal microbiota raises the possibility that microbes can sequester tryptophan from the diet, convert it to tryptamine, and thereby alter the spectrum and distribution of tryptophan metabolites that result in the host. Reducing the level of plasma tryptophan would decrease the production of serotonin in the brain and could represent one mechanism by which the microbiota influence behavior.

EXPERIMENTAL PROCEDURES

Bacterial Growth Conditions

Clostridium sporogenes ATCC 15579 was grown in reinforced clostridium medium (BD) supplemented with MEM Vitamins (GIBCO) and incubated anaerobically at 37°C. *Ruminococcus gnavus* ATCC 29149 was grown in brain heart infusion medium (BD) supplemented with yeast extract (5 g/L) and hemin (5 g/L) and incubated anaerobically at 37°C. For the qualitative cell-based decarboxylation assay, cultures were grown to stationary phase in rich medium, and the cell mass was transferred to a minimal medium (Bell, 1976) containing 5 g/L tryptophan, tyrosine, or phenylalanine. Cultures were incubated at 37°C for 24–72 hr before analysis of the culture fluid by HPLC.

Expression and Purification of CLOSP0_02083 and RUMGNA_01526

Expression constructs were transformed into *E. coli* BL21 (DE3) cells, grown to saturation in LB medium (Fisher Scientific) supplemented with kanamycin (50 µg/ml) at 37°C, and diluted 1:33 into the same medium. The expression of RUMGNA_01526 N-terminal His₆ fusion proteins was induced at OD₆₀₀ 0.6 with 1 mM isopropyl β-D-thiogalactopyranoside, and overexpression was allowed to proceed at 25°C for 16–20 hr. Cells from 1 L of culture were pelleted by centrifugation (10 min at 5200 × g), resuspended in 40 ml of buffer A (300 mM NaCl, 50 mM NaH₂PO₄, 10 mM Imidazole, pH 8.0), and lysed by passage through a cell disruptor (EmulsiFlex C3, Avestin, Ottawa) at 10,000 pounds per square inch. Cell debris was removed by centrifugation (20 min at 31,000 × g) and the supernatant was incubated with 1.5 ml of Ni-nitrilotriacetic acid resin (QIAGEN, Valencia, CA) at 4°C for 1 hr. After the unbound fraction was discarded, the resin was resuspended in 30 ml of buffer B (300 mM NaCl, 50 mM NaH₂PO₄, 20 mM Imidazole, pH 8.0), loaded onto a column, and washed with 60 ml of buffer B. Recombinant enzyme was eluted from the column with buffer C (300 mM NaCl, 50 mM NaH₂PO₄, 250 mM Imidazole, pH 8.0) and dialyzed at 4°C against 4 l of buffer D (50 mM Tris-HCl pH 7.5, 300 mM NaCl). The protein was used immediately, and a fresh batch was purified for each enzymatic assay. The concentrations of purified enzyme were determined spectrophotometrically using a Coomassie Protein Assay (Thermo Fisher). The expression of CLOSP0_02083 N-terminal His₆ fusion proteins was performed as described except for the following: LB medium was supplemented with 10 mM tryptophan and 30 µM PLP, cultures were expressed for 16–20 hr at 20°C, buffers A and D contained 30 µM PLP, and 1.0 ml of Ni-nitrilotriacetic acid resin was used.

Qualitative Cell-Based Assay for Decarboxylase Substrate Selectivity

Overnight cultures of *E. coli* BL21 (DE3) expressing pET-28a-decarboxylase constructs were diluted (1:20) into fresh LB medium containing 50 µg/ml kanamycin and grown for 90 min at 37°C. Cells were pelleted by centrifugation and resuspended in M9 minimal medium containing 5 mg/mL of tryptophan, tyrosine, or phenylalanine and 1 mM isopropyl β-D-thiogalactopyranoside. After 24 hr, 100 µl of clarified supernatant was analyzed by HPLC.

Kinetic Characterization of CLOSP0_02083 and RUMGNA_01526

Activity with Aromatic Amino Acid Substrates

Reaction mixtures contained 50 mM sodium phosphate pH 6.5, 300 mM NaCl, and 40 µM PLP. Reactions were initiated by the addition of enzyme and terminated by quenching aliquots with 1 volume of MeOH and performed at 37°C. All substrates purchased from Sigma-Aldrich. More details provided in the Supplemental Information.

X-ray Crystallography

Crystals of RUMGNA_01526 were grown at room temperature in hanging drops consisting of equal volumes (1 + 1 µl) of 10 mg/ml RUMGNA_01526 and a crystallization solution composed of 0.1 M Bicine pH 8.5 and 25% PEG 3350. Crystals of RUMGNA_01526 with (S)-α-FMT were grown at room temperature in sitting drops consisting of equal volumes of 10 mg/ml RUMGNA_01526 pre-mixed with 5 mM (S)-α-FMT and a crystallization solution composed of 30% ethoxyethanol, 0.1 M citrate pH 5.25, and 4% polypropylene P400.

Structure Determination and Refinement

Crystals were flash-frozen in liquid nitrogen with 10% glycerol supplemented as a cryoprotectant. Data were collected on beamline 8.3.1 at the Advanced Light Source (Table S1). X-ray reflections were processed using xia2. All subsequent molecular replacement and structure analysis was performed using the PHENIX software suite. For the structure of RUMGNA_01526 in its native form, a molecular replacement search ensemble was created from the homologous models 2JIS, 3RBF, 4E10, 3RCH, 2QMA, and 1JS3 using Phenix.sculptor and Phenix.ensemble. The structure of RUMGNA_01526 in its native form was used as a molecular replacement search model for the (S)-α-FMT-bound structure. All visualization components were performed using COOT.

ACCESSION NUMBERS

Coordinates in the Protein Data Bank have been deposited with accession codes 4OBU (native RUMGNA_01526) and 4OBV (RUMGNA_01526-(S)-α-FMT complex).

SUPPLEMENTAL INFORMATION

Supplemental Information includes six figures, one table, Supplemental Experimental Procedures, and Supplemental References and can be found with this article online at <http://dx.doi.org/10.1016/j.chom.2014.09.001>.

ACKNOWLEDGMENTS

We are indebted to Justin Rettenmaier for an early computational analysis of candidate decarboxylases from *Clostridium sporogenes* and to members of the Fischbach group for ideas and helpful discussions. This work was supported by a Fellowship for Science and Engineering from the David and Lucile Packard Foundation (M.A.F.), Medical Research Program Grant from the W.M. Keck Foundation (M.A.F.), DARPA award HR0011-12-C-0067 (M.A.F.), QB3 (J.S.F.), and NIH grants OD007290 and GM081879 (M.A.F.) and OD009180 (J.S.F.), as well as an HHMI Predoctoral Fellowship (P.C.) and NIH K08DK100638 (P.C.K.).

Received: May 5, 2014

Revised: July 14, 2014

Accepted: September 2, 2014

Published: September 25, 2014

REFERENCES

- Anderson, G.M. (1975). Quantitation of tryptophan metabolites in rat feces by thin-layer chromatography. *J. Chromatogr. A* 105, 323–328.
- Bell, S.M. (1976). Treatment with gentamicin monitored by serum antibiotic assay. *Med. J. Aust.* 2, 481–484.
- Bhattacharjee, M.K., and Snell, E.E. (1990). Pyridoxal 5'-phosphate-dependent histidine decarboxylase. Mechanism of inactivation by alpha-fluoromethylhistidine. *J. Biol. Chem.* 265, 6664–6668.
- Bianchetti, M.G., Minder, I., Beretta-Piccoli, C., Meier, A., and Weidmann, P. (1982). Effects of tyramine on blood pressure and plasma catecholamines in normal and hypertensive subjects. *Klin. Wochenschr.* 60, 465–470.
- Bischoff, S.C., Mailer, R., Pabst, O., Weier, G., Sedlik, W., Li, Z., Chen, J.J., Murphy, D.L., and Gershon, M.D. (2009). Role of serotonin in intestinal inflammation: Knockout of serotonin reuptake transporter exacerbates 2,4,6-trinitrobenzene sulfonic acid colitis in mice. *Am. J. Physiol. Gastrointest. Liver Physiol.* 296, G685–G695.
- Borowsky, B., Adham, N., Jones, K.A., Raddatz, R., Artymyshyn, R., Ogozalek, K.L., Durkin, M.M., Lakhani, P.P., Bonini, J.A., Pathirana, S., et al. (2001). Trace amines: identification of a family of mammalian G protein-coupled receptors. *Proc. Natl. Acad. Sci. USA* 98, 8966–8971.
- Bravo, J.A., Forsythe, P., Chew, M.V., Escaravage, E., Savignac, H.M., Dinan, T.G., Bienenstock, J., and Cryan, J.F. (2011). Ingestion of *Lactobacillus* strain regulates emotional behavior and central GABA receptor expression in a mouse via the vagus nerve. *Proc. Natl. Acad. Sci. USA* 108, 16050–16055.

- Brooks, J.B., Nunez-Montiel, O.L., Basta, M.T., and Hierholzer, J.C. (1984). Studies of stools from pseudomembranous colitis, rotaviral, and other diarrheal syndromes by frequency-pulsed electron capture gas-liquid chromatography. *J. Clin. Microbiol.* 20, 549–560.
- Burkhardt, P., Dominici, P., Borri-Voltattorni, C., Janssonius, J.N., and Malashkevich, V.N. (2001). Structural insight into Parkinson's disease treatment from drug-inhibited DOPA decarboxylase. *Nat. Struct. Biol.* 8, 963–967.
- Chander, H., Batish, V.K., Babu, S., and Singh, R.S. (1989). Factors affecting amine production by a selected strain of *Lactobacillus bulgaricus*. *J. Food Sci.* 54, 940–942.
- Clarke, G., Grenham, S., Scully, P., Fitzgerald, P., Moloney, R.D., Shanahan, F., Dinan, T.G., and Cryan, J.F. (2013). The microbiome-gut-brain axis during early life regulates the hippocampal serotonergic system in a sex-dependent manner. *Mol. Psychiatry* 18, 666–673.
- Desbonnet, L., Garrett, L., Clarke, G., Bienenstock, J., and Dinan, T.G. (2008). The probiotic *Bifidobacteria infantis*: An assessment of potential antidepressant properties in the rat. *J. Psychiatr. Res.* 43, 164–174.
- Diaz Heijtz, R., Wang, S., Anuar, F., Qian, Y., Björkholm, B., Samuelsson, A., Hibberd, M.L., Forssberg, H., and Pettersson, S. (2011). Normal gut microbiota modulates brain development and behavior. *Proc. Natl. Acad. Sci. USA* 108, 3047–3052.
- Ebeid, A.M., Smith, A., Escourrou, J., Murray, P., and Fischer, J.E. (1978). Increased immunoreactive vasoactive intestinal peptide in the cerebro-spinal fluid (CSF) of dogs and monkeys in hepatic failure. *J. Surg. Res.* 25, 538–541.
- Facchini, P.J., Huber-Allanach, K.L., and Tari, L.W. (2000). Plant aromatic L-amino acid decarboxylases: evolution, biochemistry, regulation, and metabolic engineering applications. *Phytochemistry* 54, 121–138.
- Fenalti, G., Law, R.H., Buckle, A.M., Langendorf, C., Tuck, K., Rosado, C.J., Faux, N.G., Mahmood, K., Hampe, C.S., Banga, J.P., et al. (2007). GABA production by glutamic acid decarboxylase is regulated by a dynamic catalytic loop. *Nat. Struct. Mol. Biol.* 14, 280–286.
- Fontanilla, D., Johannessen, M., Hajipour, A.R., Cozzi, N.V., Jackson, M.B., and Ruoho, A.E. (2009). The hallucinogen N,N-dimethyltryptamine (DMT) is an endogenous sigma-1 receptor regulator. *Science* 323, 934–937.
- Gallagher, T., Rozwarski, D.A., Ernst, S.R., and Hackert, M.L. (1993). Refined structure of the pyruvoyl-dependent histidine decarboxylase from *Lactobacillus 30a*. *J. Mol. Biol.* 230, 516–528.
- Gershon, M.D., and Tack, J. (2007). The serotonin signaling system: from basic understanding to drug development for functional GI disorders. *Gastroenterology* 132, 397–414.
- Giardina, G., Montioli, R., Gianni, S., Cellini, B., Paiardini, A., Voltattorni, C.B., and Cutruzzolà, F. (2011). Open conformation of human DOPA decarboxylase reveals the mechanism of PLP addition to Group II decarboxylases. *Proc. Natl. Acad. Sci. USA* 108, 20514–20519.
- Hayashi, H., Tanase, S., and Snell, E.E. (1986). Pyridoxal 5'-phosphate-dependent histidine decarboxylase. Inactivation by alpha-fluoromethylhistidine and comparative sequences at the inhibitor- and coenzyme-binding sites. *J. Biol. Chem.* 261, 11003–11009.
- Hsiao, E.Y., McBride, S.W., Hsien, S., Sharon, G., Hyde, E.R., McCue, T., Codelli, J.A., Chow, J., Reisman, S.E., Petrosino, J.F., et al. (2013). Microbiota modulate behavioral and physiological abnormalities associated with neurodevelopmental disorders. *Cell* 155, 1451–1463.
- Ishihara, A., Nakao, T., Mashimo, Y., Murai, M., Ichimaru, N., Tanaka, C., Nakajima, H., Wakasa, K., and Miyagawa, H. (2011). Probing the role of tryptophan-derived secondary metabolism in defense responses against Bipolaris oryzae infection in rice leaves by a suicide substrate of tryptophan decarboxylase. *Phytochemistry* 72, 7–13.
- Jeffery, I.B., O'Toole, P.W., Öhman, L., Claesson, M.J., Deane, J., Quigley, E.M., and Simrén, M. (2012). An irritable bowel syndrome subtype defined by species-specific alterations in faecal microbiota. *Gut* 61, 997–1006.
- John, R.A. (1995). Pyridoxal phosphate-dependent enzymes. *Biochim. Biophys. Acta* 1248, 81–96.
- Komori, H., Nitta, Y., Ueno, H., and Higuchi, Y. (2012). Structural study reveals that Ser-354 determines substrate specificity on human histidine decarboxylase. *J. Biol. Chem.* 287, 29175–29183.
- Lang, G., Kalvelage, T., Peters, A., Wiese, J., and Imhoff, J.F. (2008). Linear and cyclic peptides from the entomopathogenic bacterium *Xenorhabdus nematophilus*. *J. Nat. Prod.* 71, 1074–1077.
- Li, J., Chen, G., and Webster, J.M. (1997). Nematophin, a novel antimicrobial substance produced by *Xenorhabdus nematophilus* (Enterobactereaceae). *Can. J. Microbiol.* 43, 770–773.
- Linden, D.R., Chen, J.X., Gershon, M.D., Sharkey, K.A., and Mawe, G.M. (2003). Serotonin availability is increased in mucosa of guinea pigs with TNBS-induced colitis. *Am. J. Physiol. Gastrointest. Liver Physiol.* 285, G207–G216.
- Linden, D.R., Foley, K.F., McQuoid, C., Simpson, J., Sharkey, K.A., and Mawe, G.M. (2005). Serotonin transporter function and expression are reduced in mice with TNBS-induced colitis. *Neurogastroenterol. Motil.* 17, 565–574.
- Lundgren, O. (1998). 5-Hydroxytryptamine, enterotoxins, and intestinal fluid secretion. *Gastroenterology* 115, 1009–1012.
- Mawe, G.M., Coates, M.D., and Moses, P.L. (2006). Review article: intestinal serotonin signalling in irritable bowel syndrome. *Aliment. Pharmacol. Ther.* 23, 1067–1076.
- Marcobal, A., Kashyap, P.C., Nelson, T.A., Aronov, P.A., Donia, M.S., Spormann, A., Fischbach, M.A., and Sonnenburg, J.L. (2013). A metabolomic view of how the human gut microbiota impacts the host metabolome using humanized and gnotobiotic mice. *ISME J.* 7, 1933–1943.
- Mayer, E.A. (2011). Gut feelings: the emerging biology of gut-brain communication. *Nat. Rev. Neurosci.* 12, 453–466.
- Ormsbee, H.S., 3rd, and Fondacaro, J.D. (1985). Action of serotonin on the gastrointestinal tract. *Proc. Soc. Exp. Biol. Med.* 178, 333–338.
- Proschak, A., Schultz, K., Herrmann, J., Dowling, A.J., Brachmann, A.O., ffrench-Constant, R., Müller, R., and Bode, H.B. (2011). Cytotoxic fatty acid amides from *Xenorhabdus*. *ChemBioChem* 12, 2011–2015.
- Schneider, G., Käck, H., and Lindqvist, Y. (2000). The manifold of vitamin B6 dependent enzymes. *Structure* 8, R1–R6.
- Sudo, N., Chida, Y., Aiba, Y., Sonoda, J., Oyama, N., Yu, X.N., Kubo, C., and Koga, Y. (2004). Postnatal microbial colonization programs the hypothalamic-pituitary-adrenal system for stress response in mice. *J. Physiol.* 558, 263–275.
- Takaki, M., Mawe, G.M., Barasch, J.M., Gershon, M.D., and Gershon, M.D. (1985). Physiological responses of guinea-pig myenteric neurons secondary to the release of endogenous serotonin by tryptamine. *Neuroscience* 16, 223–240.
- Turvill, J.L., Connor, P., and Farthing, M.J. (2000). The inhibition of cholera toxin-induced 5-HT release by the 5-HT(3) receptor antagonist, granisetron, in the rat. *Br. J. Pharmacol.* 130, 1031–1036.
- van Poelje, P.D., and Snell, E.E. (1990). Pyruvoyl-dependent enzymes. *Annu. Rev. Biochem.* 59, 29–59.
- Wikoff, W.R., Anfora, A.T., Liu, J., Schultz, P.G., Lesley, S.A., Peters, E.C., and Siuzdak, G. (2009). Metabolomics analysis reveals large effects of gut microflora on mammalian blood metabolites. *Proc. Natl. Acad. Sci. USA* 106, 3698–3703.
- Yuwen, L., Zhang, F.L., Chen, Q.H., Lin, S.J., Zhao, Y.L., and Li, Z.Y. (2013). The role of aromatic L-amino acid decarboxylase in bacillamide C biosynthesis by *Bacillus atrophaeus* C89. *Sci. Rep.* 3, 1753.
- Zucchi, R., Chiellini, G., Scanlan, T.S., and Grandy, D.K. (2006). Trace amine-associated receptors and their ligands. *Br. J. Pharmacol.* 149, 967–978.

Cell Host & Microbe, Volume 16

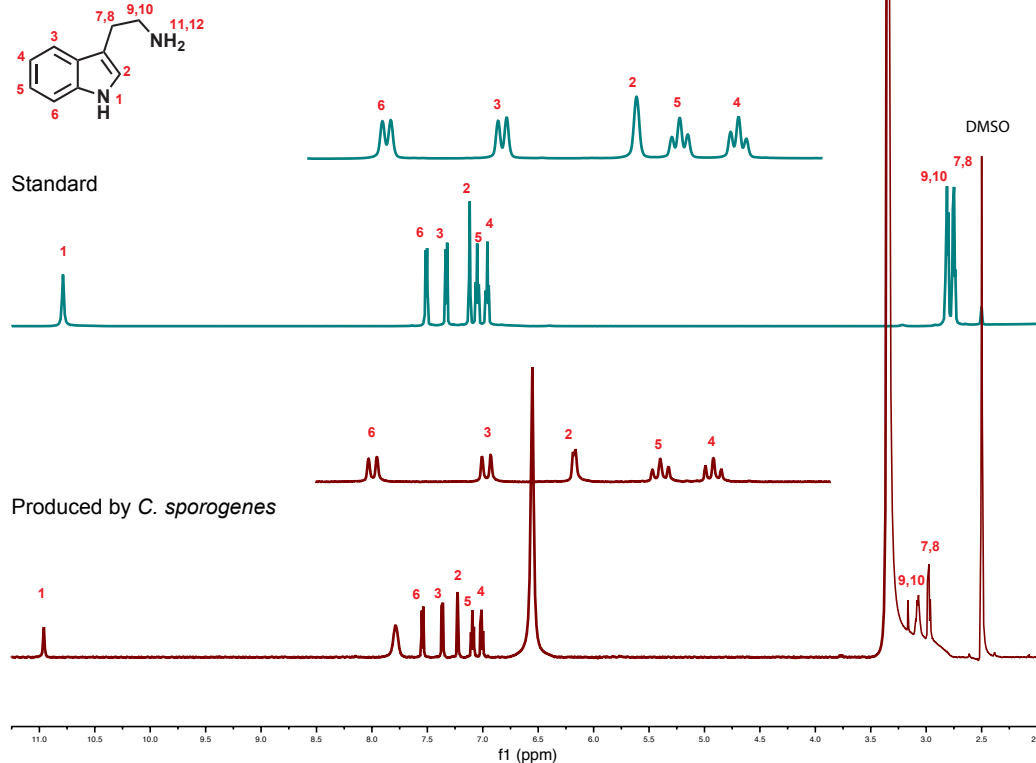
Supplemental Information

**Discovery and Characterization of
Gut Microbiota Decarboxylases that Can
Produce the Neurotransmitter Tryptamine**

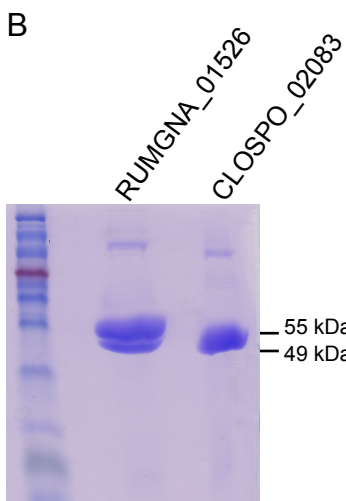
Brianna B. Williams, Andrew H. Van Benschoten, Peter Cimermancic, Mohamed S. Donia, Michael Zimmermann, Mao Takeuchi, Atsushi Ishihara, Purna C. Kashyap, James S. Fraser, and Michael A. Fischbach

Figure S1

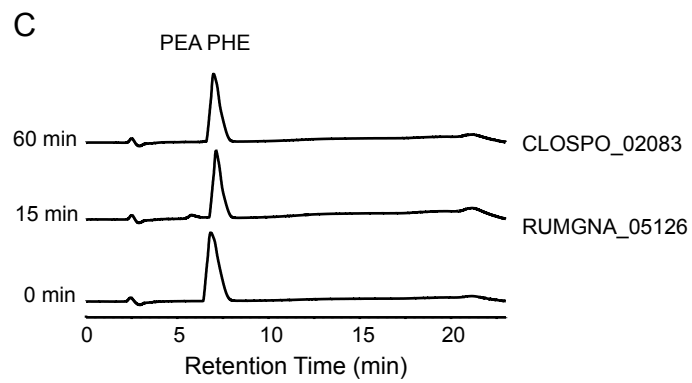
A



B



C



D

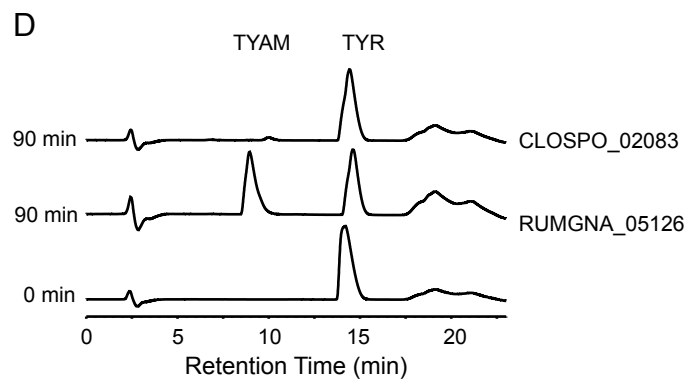
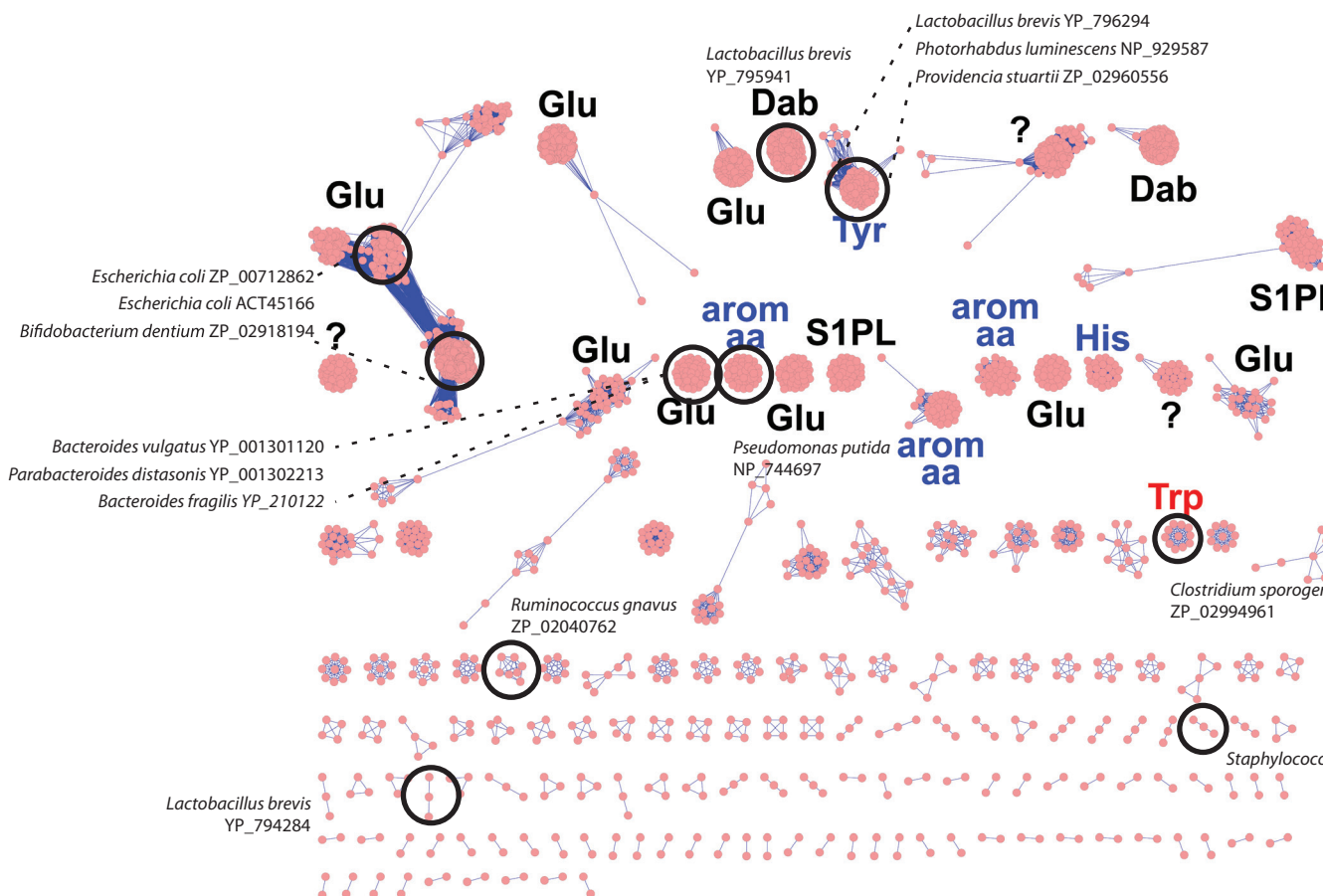


Figure S2

A



B

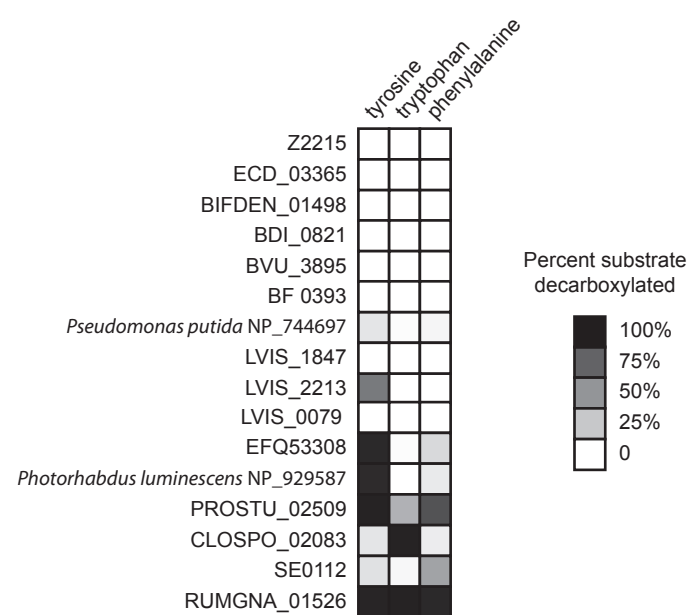


Figure S3**A**

	CLOSPO_02083 Tryptophan	RUMGNA_01526 Tryptophan	RUMGNA_01526 Phenylalanine
K_m (mM)	2.8 ± 0.03	1.1 ± 0.07	70 ± 6.6
V_{max} (mM/min)	0.12 ± 0.00	0.04 ± 0.00	0.12 ± 0.01
k_{cat} (min ⁻¹)	1200	4400	230
k_{cat}/K_m (M ⁻¹ sec ⁻¹)	7.3×10^3	6.8×10^4	56

B

	CLOSPO_02083 Tryptophan	RUMGNA_01526 Tryptophan	RUMGNA_01526 Phenylalanine
$K_{0.5}$ (mM)	2.13 ± 0.03	0.76 ± 0.03	23 ± 1.2
V_{max} (mM/min)	0.11 ± 0.00	0.04 ± 0.00	0.06 ± 0.00
h	1.5	1.7	2.7

C

RUMGNA_01526 progress curve

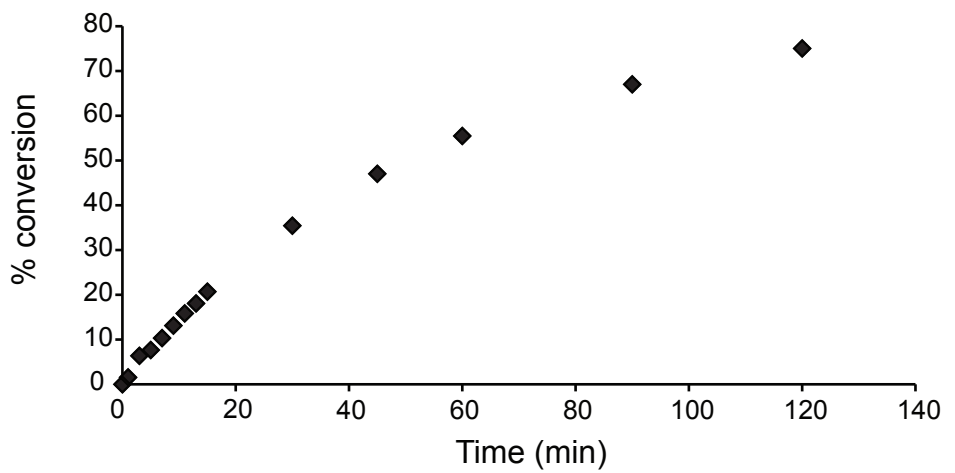


Figure S4

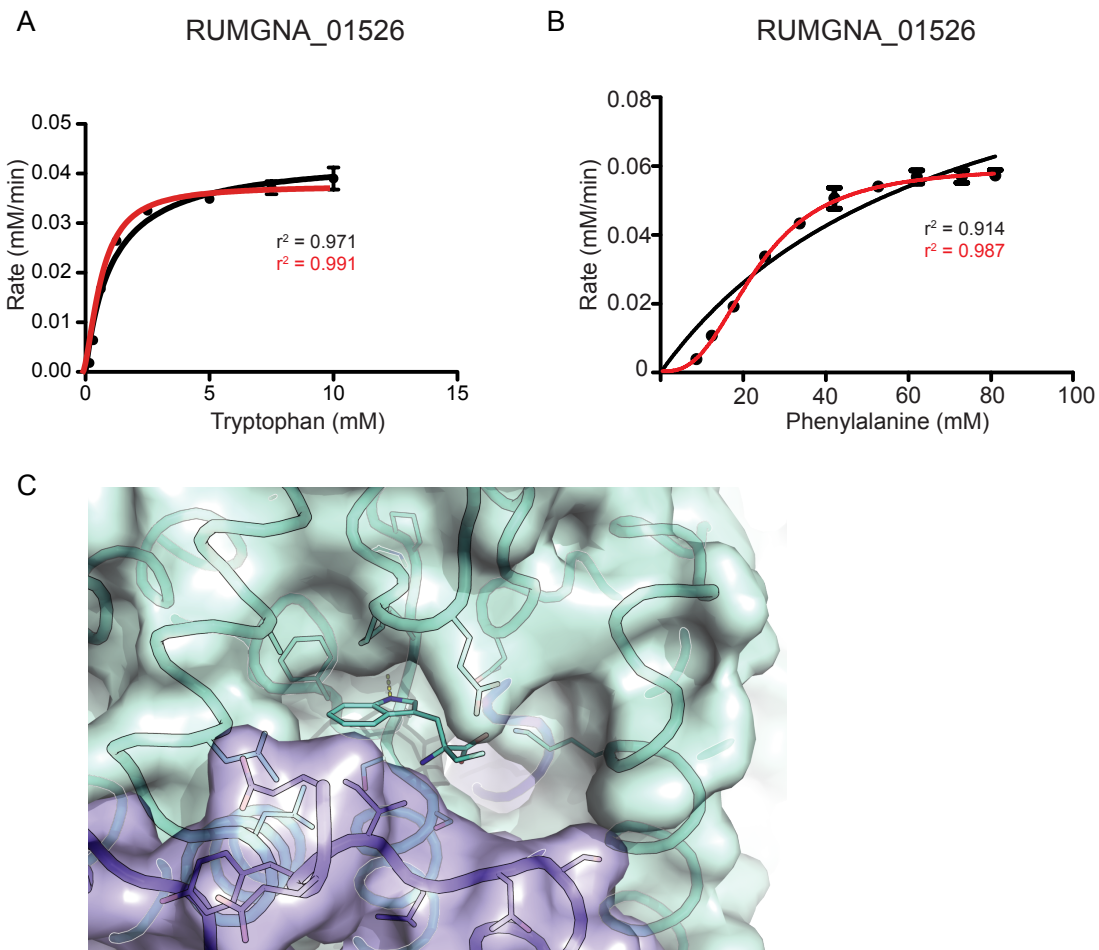


Figure S5

Tryptamine stimulation of ion secretion in colonic epithelia

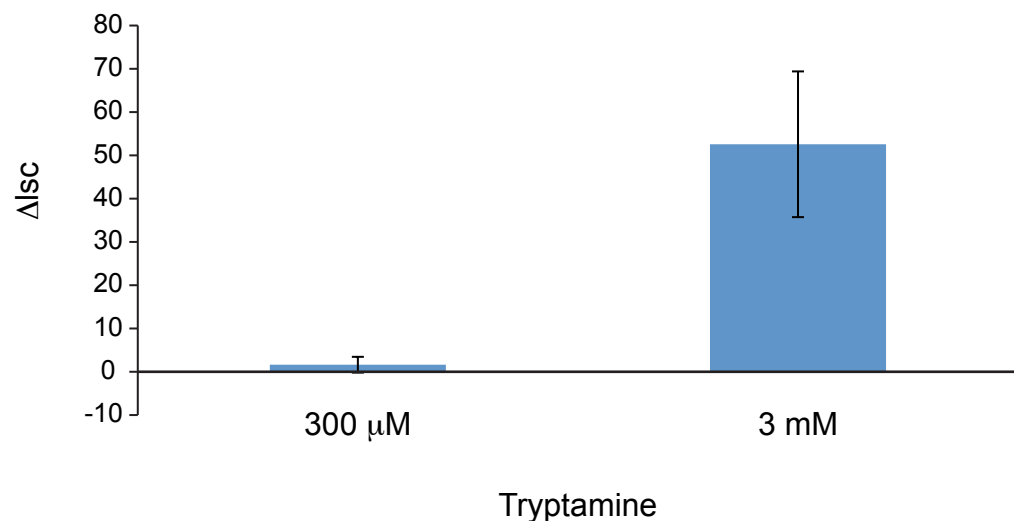
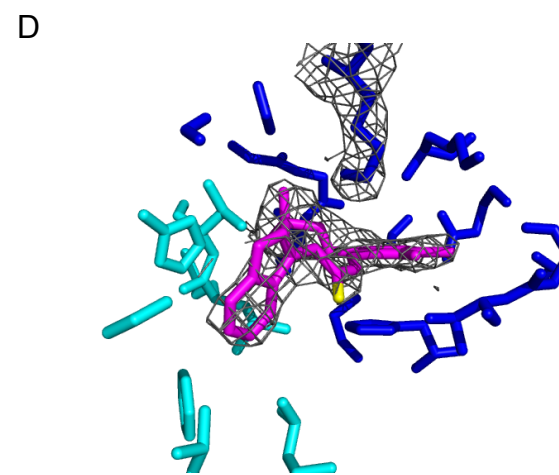
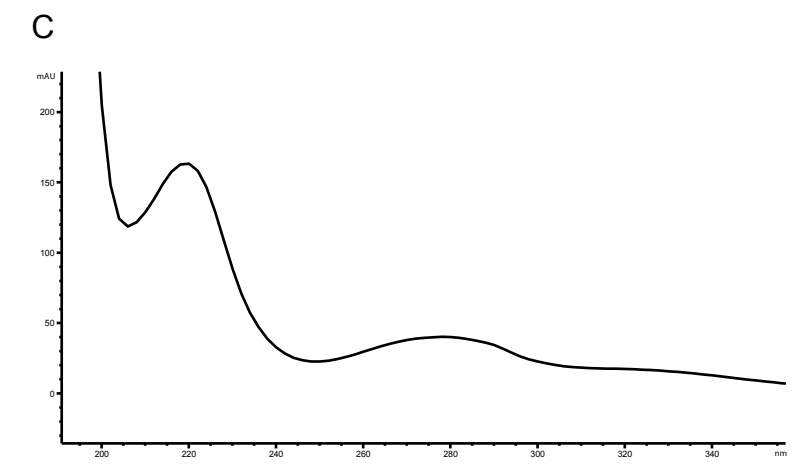
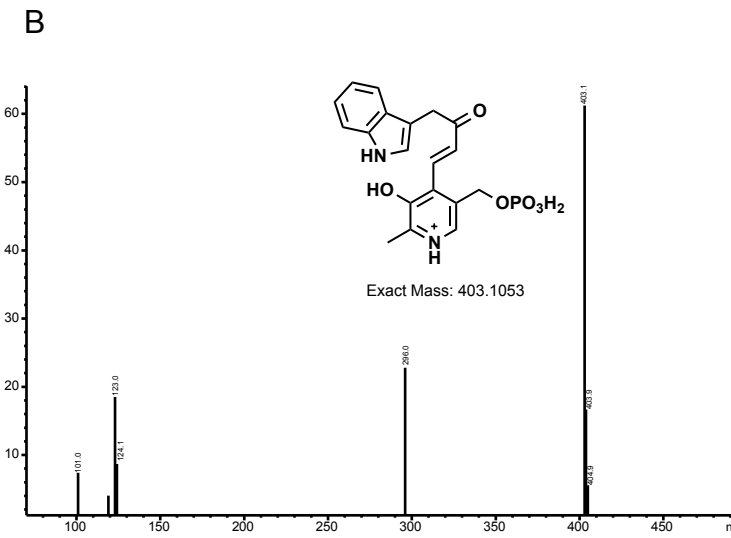
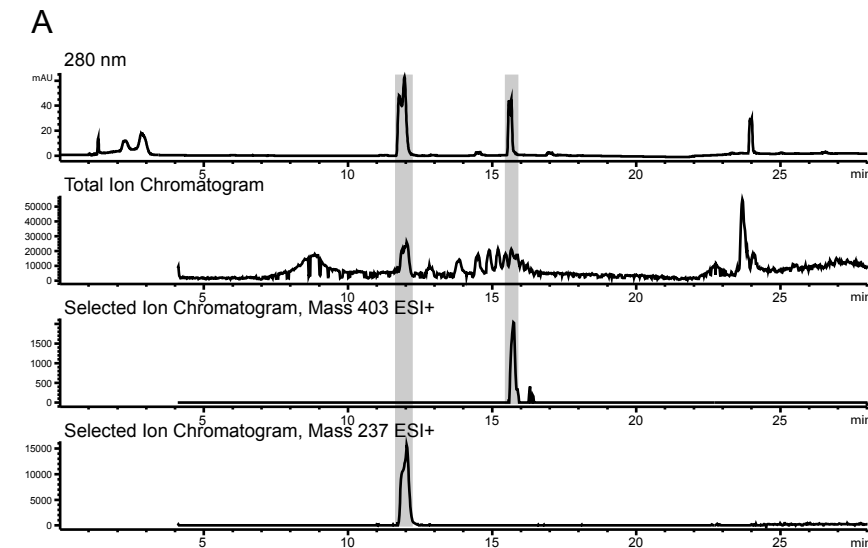


Figure S6

Supplemental Figure Legends

Figure S1 related to Figure 1. Characterization of tryptamine production. (A) NMR of *C. sporogenes* produced tryptamine compared to standard (Sigma-Aldrich). Standard tryptamine is shown in teal, and *C. sporogenes*-produced tryptamine is shown in burgundy. (B) SDS-PAGE of purified CLOSPO_02083 and RUMGNA_01526. Using a BioRad ReadyGel, Precast SDS-PAGE 10% Tris-HCl, 1 μ L of purified protein was loaded. Lane 1: Precision Plus Protein Prestained Standards, Dual Color, Lane 2: RUMGNA_01526 55 kDa, Lane 3: CLOSPO_02083 49 kDa. (C, D) Biochemical activity of CLOSPO_02083 and RUMGNA_01526 with phenylalanine and tyrosine substrates. HPLC traces for (C) phenylalanine or (D) tyrosine decarboxylation by CLOSPO_02083 or RUMGNA_01526.

Figure S2 related to Figure 2. Cytoscape clustering of pfam00282 containing sequences in the JGI database and activity of selected enzymes. (A) The pfam consensus sequence for PLP-dependent decarboxylases (PLP_dec, pfam00282) was used as a query in a BLAST search against the JGI database and hits were clustered based on similarity. Clusters are labeled with predicted substrates. Genes included in this study were selected to represent several clusters and are labeled. (B) Summary of decarboxylase activity. Genes were cloned into pET-28a and expressed in *E. coli* BL21 in the presence of tryptophan, tyrosine, or phenylalanine for 24 hours. Percent decarboxylation was determined by dividing the integrated peak area (AUC) of the amine by the sum of the AUC of both the amine and acid, and represented in gray scale.

Figure S3 related to Figure 4. Table of kinetic results. (A) Michaelis-Menten and (B) Hill equation kinetic parameters for CLOPSO_02083 and RUMGNA_01526 with tryptophan and

RUMGNA_01526 with phenylalanine. (C) Progress curve of tryptophan consumption by 10 nM RUMGNA_01526 in the presence of 1.25 mM tryptophan.

Figure S4 related to Figure 3. Hill equation fit to RUMGNA_01526 kinetic data. Rate (mM tryptamine/min) vs substrate concentration curves for (A) tryptophan or (B) phenylalanine decarboxylation by RUMGNA_01526 100 nM enzyme incubated with tryptophan varied from 0.15-24.5 mM. GraphPad was used to fit the Michaelis-Menten (black) and Hill (red) equations. (C) Allosteric site shows free (S)- α -FMT buried in a hydrophobic pocket near the N-terminus of the enzyme.

Figure S5 related to Figure 1. Tryptamine stimulates ion secretion by intestinal epithelial cells. Segments of proximal-mid colon, stripped of external muscle layers, were exposed to either 300 μ M or 3 mM tryptamine using the Ussing chamber. The change in short circuit current was determined. A significant increase in ion secretions was observed in the presence of 3 mM but not 300 μ M tryptamine.

Figure S6 related to Figure 3. Structure determination of (S)- α -FMT-PLP adduct (A) 280 nm UV trace, total ion chromatogram, and selected ion chromatograms for the released adduct. (B) Mass spectrum of adduct shows a compound with a mass of 403, corresponding to the structure shown in the inset. (C) UV-Vis spectrum of adduct. (D) Electron density shows clear separation of adduct and lysine residue.

Table S1 related to Figure 3 Data collection and refinement statistics

	Apo-RUMGNA_01526	S-aFMT-RUMGNA_01526
Wavelength (Å)		
Resolution range (Å)	79.37 - 2.804 (2.905 - 2.804)	52.44 - 2.84 (2.942 - 2.84)
Space group	P 1	P 41 21 2
Unit cell	58.63 145.77 165.07 72.85 88.84 88.3	135.03 135.03 249.8 90 90 90
Total reflections	218936 (22174)	730528 (73919)
Unique reflections	121102 (12262)	55248 (5448)
Multiplicity	1.8 (1.8)	13.2 (13.6)
Completeness (%)	94.70 (96.28)	99.97 (99.96)
Mean I/sigma(I)	9.54 (2.09)	25.80 (3.80)
Wilson B-factor	41.16	54.76
R-merge	0.08033 (0.363)	0.119 (0.8652)
R-meas	0.1136	0.1238
CC1/2	0.99 (0.73)	0.999 (0.881)
CC*	0.998 (0.919)	1 (0.968)
R-work	0.2311 (0.3077)	0.2098 (0.2745)
R-free	0.2568 (0.3623)	0.2423 (0.3494)
Number of atoms	29598	15146
macromolecules	29064	14886
ligands	120	184
water	414	0
Protein residues	3696	1889
RMS(bonds)	0.002	0.007
RMS(angles)	0.67	0.64
Ramachandran favored (%)	96	95
Ramachandran outliers (%)	0	0.053
Clashscore	3.03	3.04
Average B-factor	21.2	36.4
macromolecules	21.3	36.2
ligands	41.8	47.9
solvent	9.7	
Statistics for the highest-resolution shell are shown in parentheses.		

Experimental Procedures

Cloning candidate decarboxylase genes. Candidate decarboxylase genes were cloned from genomic DNA prepared from each strain using Phusion High Fidelity DNA Polymerase (NEB). PCR products were purified (MinElute, Qiagen) and used directly as primers in a CPEC reaction with pET-28a (Novagen) that had previously been digested with *Nde*I and *Xho*I (98°C for 30 s; 6 cycles of 98°C for 10 s, 55°C for 30 s, 72°C for 3 min; 72°C for 5 min). The identities of the resulting pET-28a-decarboxylase constructs were confirmed by DNA sequencing.

HPLC analysis of culture fluid from *E. coli* expressing putative decarboxylases. Samples of cell-free supernatant containing tryptophan, phenylalanine, or tyrosine were analyzed on an Agilent 1200 series HPLC equipped with a diode array detector using a ThermoScientific Hypercarb column (100 mm x 4.6 mm x 5 µm) at a flow rate of 1.0 ml/min at ambient temperature. There were four mobile phase solvents: (A) water, (B) acetonitrile, (C) isopropanol, and (D) methanol, each supplemented with 0.1% TFA (trifluoroacetic acid). The elution gradient had the following profile: 5.0-30.8% B, 5.0-30.8% C, and 2.0% D from 0-14 min; 30.8-49.0% B, 30.8-49.0% C, 2.0% D from 14-17 min; and 49.0-5.0% B, 49.0-5.0% C, 2.0% D from 17-20 min;

5.0% B, 5.0% C, 2.0% D from 20-23 min. Standard elution times were as follows: tryptophan 13.0 min (monitored at 280 nm), tryptamine 11.0 min (280 nm); phenylalanine 6.9 min (220 nm), phenethylamine 5.6 min (220 nm), tyrosine 6.8 min (220 nm), tyramine 5.1 min (220 nm).

Kinetic characterization of CLOSPO_02083 and RUMGNA_01526 activity with aromatic amino acid substrates. Reaction mixtures contained 50 mM sodium phosphate pH 6.5, 300 mM NaCl, and 40 μ M PLP. Reactions were initiated by the addition of enzyme and terminated by quenching aliquots with 1 volume of MeOH and performed at 37°C. All substrates purchased from Sigma-Aldrich.

To determine the kinetic parameters for the decarboxylation of tryptophan by RUMGNA_01526, RUMGNA_01526 was added to a final concentration of 10 nM, and k_{cat} and K_m were determined by varying the concentration of tryptophan from 0.15-10 mM. Reactions proceeded for 7 min and were quenched as described. 100 μ l of the quenched reaction was analyzed by HPLC. Peak areas were integrated and compared with a standard curve to calculate product concentration. Triplicate measurements were made from a single batch of purified enzyme. Initial velocity data were fit to the Michaelis-Menten equation by using the program GraphPad. The allosteric sigmoidal model was used by fitting to the Hill equation: $y=v_{max}^*x^h/(K_{0.5}^h+x^h)$, where h is the Hill coefficient and $K_{0.5}$ is the apparent concentration at half maximal velocity.

Under the same buffer and reaction conditions, the kinetic parameters for the decarboxylation of phenylalanine by RUMGNA_01526 were determined by adding RUMGNA_01526 to a final concentration of 500 nM and the concentration of phenylalanine varied from 5-80 mM. Reactions proceeded for 10 min. The kinetic parameters for the decarboxylation of tryptophan by CLOSPO_02083 were determined by adding CLOSPO_02083 to a final concentration of 100 nM and the concentration of tryptophan varied from 0.15-24.5

mM; reactions proceeded for 6 minutes. Decarboxylation of phenylalanine by CLOSPO_02083 was not observed under saturation conditions using 1 μ M enzyme and 90mM substrate for 60 minutes. Decarboxylation of tyrosine by RUMGNA_01526 and CLOSPO_02083 was observed using 1 μ M enzyme with 2.28 mM tyrosine for 90 minutes.

Experiments with the inhibitor (S)- α -FMT were performed by analyzing product formation over time after the addition of (S)- α -FMT to pre-incubated enzyme and substrate at a concentration of 3^*K_m (2.5 mM Trp for RUMGNA_01526, and 10 mM Trp for CLOSPO_02083). Progress curves were fitted to the equation $[P]=(v_i/k_{obs})(1-exp(-k_{obs}t))$, where P is the product formed at time t , v_i is the initial velocity, and k_{obs} is the apparent first-order rate constant for enzyme inactivation. The k_{obs} were plotted versus inhibitor concentration and fitted to the equation $k_{obs}=k_{inact}[I]/(K_{app}+[I])$, where K_{app} is the apparent dissociation constant of the reversible enzyme-inhibitor complex, and k_{inact} is the first-order rate constant for apparent irreversible conversion of the enzyme-inhibitor complex to covalently bound complex. K_i values were calculated using the equation $K_i=K_{app}/(1+[tryptophan])/K_{m,Trp})$ using experimentally determined K_m values for tryptophan (32).

Ion secretion from the murine colon. A segment of proximal-mid colon, stripped of external muscle layers from each of three SvEv129 mice was mounted in 0.3 cm² area, 4 mL Ussing chamber. Change in short circuit current (Δ Isc) was determined in response to two concentrations of tryptamine (300 μ M and 3mM) on the mucosal side to mimic bacterially produced tryptamine.

Phylogenetic analysis of microbial decarboxylases. Multiple sequence alignments were generated using MAFFT server (33), using Mafft-homologs function and the Blosum62 scoring matrix. Additionally, we used a structure-based sequence alignment of four decarboxylases (the holo structure of RUMGNA_01526 presented here and the following three structures from the:

3F9T, 3FZ8, and 4E1O) as a constraint in the alignment procedure. The structure-based sequence alignment was generated by “Match->Align” function in Chimera (34), followed by manual refinement. The phylogenetic tree was generated using the PHYLIP Neighbor Joining method (<http://evolution.genetics.washington.edu/phylip.html>), with the Jones-Taylor-Thornton distance matrix model.

Metagenomic analysis of decarboxylase prevalence. Protein databases of all assembled metagenomic data of the Human Microbiome Project stool samples were accessed through HMP Data Analysis and Coordination Center. BLASTP searches were performed using RUMGNA_01526 and CLOSPO_02083 as query sequences, with a cutoff expectation value of $1e^{-50}$ in protein sequences bigger than 100 amino acids. Hits were then analyzed further by comparing them to the NCBI protein database using BLASTP and determining their closest homologs in sequenced microbial genomes.

Supplemental References

32. Schirmer A, Kennedy J, Murli S, Reid R, & Santi DV (2006) Targeted covalent inactivation of protein kinases by resorcylic acid lactone polyketides. *Proc Natl Acad Sci USA* 103(11): 4234-4239.
33. Katoh K & Standley DM (2014) MAFFT: iterative refinement and additional methods. *Methods in molecular biology* 1079:131-146.
34. Pettersen EF, et al. (2004) UCSF Chimera--a visualization system for exploratory research and analysis. *Journal of computational chemistry* 25(13):1605-1612.